

2022

Custom biomineral production using synthetic embryonic tissue

<https://hdl.handle.net/2144/45234>

"Downloaded from OpenBU. Boston University's institutional repository."

BOSTON UNIVERSITY
GRADUATE SCHOOL OF ARTS AND SCIENCES

Thesis

**CUSTOM BIOMINERAL PRODUCTION USING SYNTHETIC
EMBRYONIC TISSUE**

by

YI CAO

B.A., Boston University, 2021

Submitted in partial fulfillment of the
requirements for the degree of
Master of Science

2022

Approved by

First Reader

Cynthia Bradham, Ph.D.
Associate Professor of Biology

Second Reader

Kimberly McCall, Ph.D.
Professor and Chair of Biology

Third Reader

Zeba Wunderlich, Ph.D.
Assistant Professor of Biology

ACKNOWLEDGEMENTS

I want to first thank these three smart, independent, and beautiful women without whom I never would have made it here:

To my advisor, professor, and friend, Cyndi, thank you for your generous sharing of knowledge and continuous support, for trusting me with this project, for teaching me not only how to do science, but also about courage and persistence in facing all kinds of unexpected blows in life. This thesis would not be possible without your guidance.

To my mom, thank you for insisting on sending me abroad and choosing the right way instead of the easy way. No words can describe how much I admire your ceaseless passion for new adventures and optimism in front of any challenges. You are forever my superwoman.

To my host mom, Liz, thank you for inviting me to the family, treating me like a real daughter, and showing me colors in life that I have never seen before. The love and care from you and everyone in the family make this foreign country ever so like home.

Thank you to my amazing labmates: James, for always knowing everything when I have a question; Nahomie, for checking on my nutritional intake and sharing your cheerful energy; Chris, for being a patient listener and always warming my heart with your thoughtful words; Dakota, for being cool as you are; Alex, for acknowledging my fashion and the beautiful time turner; Abbie, my mentor, for teaching me hand by hand about lab, devoting your time to helping with the project, and always having my back; Kelley, for making my every jump scare successful, doing weird dances with me, and

always coming to my rescue. Research was not easy, but you guys were always there to help me problem solve and lift me up with your tender encouragement.

Thank you to my committee, Dr. McCall and Dr. Wunderlich, for sharing your valuable insights in creating this thesis; to Dr. Wikramanayake and Dr. Eyckmans, for sharing your expertise in collaboration with the project; to Todd, for help with the confocal; to Pete, for taking care of our inquiries. Special thanks to Jen and Eliza for your administrative support.

Lastly, I want to thank all the professors, staff, teaching fellows, classmates, and friends that have contributed to my unforgettable memories at BU and my growth as both a scientist and an individual over the past five years. I am beyond grateful for all of you.

**CUSTOM BIOMINERAL PRODUCTION USING SYNTHETIC
EMBRYONIC TISSUE**

YI CAO

ABSTRACT

Continuous efforts have been directed towards controlled calcium carbonate biomineral synthesis in recent years. Compared to their inorganic counterparts, biominerals are more tensile in industrial applications, biocompatible with scientific designs, and sustainable for the environment. Most current approaches for synthetic biomineral production rely heavily on sophisticated engineering techniques to constrain the physical property of their crystals, which limits the adaptability of these products. Here, we proposed a novel approach to synthesize calcium carbonate biominerals by reproducing skeletogenesis of the sea urchin larva *in vitro* using common cellular and molecular methods. Skeleton formation in *Lytechinus variegatus* sea urchin embryos is a highly coordinated event, where ectodermal cells in different domains express distinct patterning cues that are received by adjacent primary mesenchyme cells (PMCs), which in turn secrete the skeleton. Our group and others have identified a range of skeletal patterning cues, and based on our current understanding of the mechanism, we envisioned a synthetic ectoderm culture using defined ectodermal lineages that, when combined with PMCs, will direct the synthetic production of skeletal structures. Here we have developed a detailed protocol for establishing such as ectoderm culture and have begun initial experiments towards this goal. Future deployment of this protocol will provide invaluable insights into the mechanism of skeletal patterning in sea urchins, as well as an

unprecedented system for customized synthetic calcium carbonate biomineral production. Finally, improving our mechanistic understanding of skeletal patterning in echinoderms has the potential to shed light on analogous biomineralization processes in other species as well.

TABLE OF CONTENTS

	Page
ACKNOWLEDGEMENTS	IV
ABSTRACT	VI
TABLE OF CONTENTS	VIII
LIST OF FIGURES	IX
LIST OF ABBREVIATIONS	X
INTRODUCTION	1
MATERIALS AND METHODS	7
RESULTS	12
DISCUSSION	20
BIBLIOGRAPHY	39
CURRICULUM VITAE	44

LIST OF FIGURES

		Page
Figure 1	PMCs secrete the larval skeleton in 1° and 2° patterning stages after gastrulation	25
Figure 2	PMCs diversify their gene expression profiles during skeletal patterning	27
Figure 3	A model for early skeletal patterning	28
Figure 4	The proposed synthetic ectoderm and PMC culture approach	29
Figure 5	Confirmation and stamping of hyalin protein	30
Figure 6	The proposed workflow to generate the cell types for the synthetic system	31
Figure 7	Preparation of <i>Axin</i> and <i>Nodal</i> mRNAs for microinjection	32
Figure 8	Gene overexpression produces the expected phenotypes	33
Figure 9	The proposed strategy to confirm cell identities using established molecular markers of ectoderm cell types	35
Figure 10	The proposed plating approach using disaggregated ectoderm cells and hyalin	36
Figure 11	Proposed approach for the synthetic complex ectoderm culture	37

LIST OF ABBREVIATIONS

ACC	amorphous calcium carbonate
ANE	anterior neuroectoderm
OA	oral-aboral
AP	anterior-posterior
AV	animal-vegetal
BE	border ectoderm
chd	chordin
cWnt	Wnt/ β -catenin
DEPC	diethyl pyrocarbonate
DV	dorsal-ventral
DVM	dorsal-ventral margin
ECM	extracellular matrix
EMT	epithelial-mesenchymal transition
FBS	fetal bovine serum
FISH	fluorescent <i>in situ</i> hybridization
GOF	gain-of-function
GRN	gene regulatory network
gsc	goosecoid
HA	hyaline layer
HEM	hyaline extraction medium
hpf	hours post fertilization

kb	kilobase
LOF	loss-of-function
LOX	5-lipoxygenase
Lv	<i>Lytechinus variegatus</i>
PABA	para-aminobenzoic acid
Pks2	Polyketide-synthase 2
PMCs	primary mesenchyme cells
qPCR	quantitative polymerase chain reaction
ser	serotonin
SLC	sulfate transporter SLC26a2/7
Sp	<i>Strongylocentrotus purpuratus</i>
SPGs	sulfated proteoglycans
synB	synaptotagmin B
TMRM	Tetramethylrhodamine, methyl ester
VEGF	vascular endothelial growth factor
VL	ventrolateral
VLCs	ventrolateral clusters
VM	ventromedial
VTs	ventral transverse rods
WMISH	whole mount <i>in situ</i> hybridization

INTRODUCTION

Specification of Body Axis

Sea urchins have long been regarded as a suitable model for the study of cell signaling during embryonic development due to their generally-high fecundity, rapid development, and well-characterized gene regulatory network (GRN) models that describe specification in the early embryo. The establishment of their two major body axes, anterior-posterior (AP), or animal-vegetal (AV) axis and dorsal-ventral (DV), also referred to as oral-aboral (OA) axis, exemplifies territorial specification based on morphogen gradients and antagonism in cell signaling. Following the autonomous activation of the canonical Wnt/ β -catenin (cWnt) pathway and nuclearization of β -catenin in the vegetal cells, the diffusion of Wnt signals towards the animal pole sets up a signaling gradient that defines the AV axis as well as specifying the three germ layers (Kipryushina and Yakovlev, 2020; Logan et al., 1999). Shortly after these events, the expression of Nodal in presumptive ventral ectoderm and the subsequent induction of Lefty and BMP2/4 initiates the establishment of the DV axis. The long-range diffusion of Lefty antagonizes Nodal on the dorsal side, leaving BMP2/4 to establish the dorsal ectodermal identity (Angerer and Angerer, 2000; Duboc et al., 2004; Duboc et al., 2008).

Primary Mesenchyme Cells

Skeletogenesis is a crucial event during the development of *Lytechinus variegatus* (Lv) embryos, during which approximately 60 PMCs migrate into distinct patterns and secrete amorphous calcium carbonate (ACC) that later transforms, in part via dehydration, into the calcite crystalline skeleton of sea urchin larvae (Beniash et al.,

1997; Beniash et al., 1999; Lyons et al., 2014). It takes approximately 48 hours for Lv embryos to develop from fertilization to late pluteus stage with a mature 4-arm skeleton (Fig. 1A). Shortly before gastrulation, PMCs undergo an epithelial–mesenchymal transition (EMT), where they gain motility to ingress into the blastocoel in preparation for their subsequent migration on the basal membrane (Fink and McClay, 1985). From there, they first migrate to a ring-and-cord pattern (Fig. 1B2) and form bilateral ventrolateral clusters (VLCs) of PMCs at the intersection of border ectoderm (BE), induced by a short-range expression of endodermal Wnt5 signals, and dorsal-ventral margin (DVM) (McIntyre et al., 2013; McIntyre et al., 2014).

The skeleton is initiated as bilateral triradiate structures within each VLC (Fig. 1B3). Current studies have identified vascular endothelial growth factor (VEGF) as a necessary and sufficient signal for the formation of skeletal triradiates by VLCs (Duloquin et al., 2007). VEGF is expressed by the ectoderm adjacent to the VLC of PMCs, and is required for their formation, while the receptor for VEGF, VEGFR, is expressed by all PMCs (Duloquin et al., 2007; Adomako-Ankomah and Etensohn, 2013). The primary skeleton is secreted in a pattern that matches the ring-and-cords arrangement of the PMCs (Fig. 1B4, blue), after which they migrate again to extend the secondary skeleton to produce the 4-arm larval skeleton, whose long posterior arms and anterior structures arise from secondary patterning (Fig. 1C2, 1C4 red).

The highly orchestrated movement of PMCs is directed by signals sent from adjacent ectodermal cells (Armstrong et al., 1993; Piacentino et al., 2016). Recombinant embryos generated from transplantation of donor PMCs to control hosts have shown that

the migration of PMCs during development results from their reception of ectodermal cues (Armstrong et al., 1993; Piacentino et al., 2016). This conclusion is reinforced by other PMC transplantation experiments that showed skeletal patterning was normal in embryos that contained an abnormal number of PMCs, or PMCs of heterochronic age (Ettensohn, 1990), suggesting that the PMC migration pattern is externally controlled rather than autonomous. Finally, PMCs produce numerous filopodial extensions as they migrate that interact with the ectoderm; these filopodia are dramatically perturbed in embryos in which skeletal patterning is abnormal (Miller et al., 1995), which indicates that these filopodia sense ectodermal cues. The PMC population diversifies during skeletogenesis, such that PMCs located in different regions of the primary and secondary PMC spatial patterns express distinct genes, shown by whole mount *in situ* hybridizations (WMISH) (Sun and Ettensohn, 2014) and fluorescent *in situ* hybridizations (FISH) coupled with PMC immunostaining (Zuch and Bradham, 2019) (Fig. 2A-C). Our unpublished results suggest that these genes are induced by the differential reception of ectodermal cues by PMCs positioned near different regions of the ectoderm. Accumulating evidence therefore points to a model that during migration, PMCs extend thin filopodia to receive local patterning cues from the nearby ectoderm, after which they diversify, then secrete calcite for the corresponding regional part of larval skeleton (Fig. 2D).

Ectodermal Cues in Skeletal Patterning

Numerous skeletal patterning cues of ectoderm origin have been identified by previous studies. Genes with obviously fluctuating expression during development were

picked out from molecular measures such as sequencing and quantitative polymerase chain reaction (qPCR). Loss-of-function (LOF) and gain-of-function (GOF) experiments were subsequently performed on these selected genes in order to examine their specific role in cell signaling and skeletal patterning. During the primary phase of skeletal patterning, the ventrolateral (VL) ectoderm adjacent to the PMC clusters expresses VEGF as described above (Fig. 3, cyan) that directs PMCs clusters and triradiate formation (Adomako-Ankomah and Etensohn, 2013; Duloquin et al., 2007). The ventral ectoderm, comprised of VL and ventromedial (VM) ectoderm, expresses the sulfate transporter SLC26a2/7 (SLC), which is necessary for the production of sulfated proteoglycans (SPGs) that are in turn required to direct ventral PMC migration but not for biomineralization or triradiate formation (Piacentino et al., 2016) (Fig. 3, blue and cyan). Each of these genes is expressed and functional prior to 18 hours post fertilization (hpf). The VL ectoderm also expresses 5-Lipoxygenase (LOX) beginning at 18 hpf (Fig. 3, purple), which regulates triradiate orientation (Zuch et al., 2022). LOX catalyzes the production of 5(S)-HETE, which exhibits chemoattractant activity on PMCs *in vitro* (Zuch et al., 2022). At later time points, the LOX expression domain expands to cover both the VL and VM ectoderm (Fig. 3, purple). Biomineralization of ventral transverse rods (VTs) by the ventral PMCs requires LOX activity during this interval, and thus presumably from VM ectoderm (Fig. 3, purple). However, LOX activity is not required for triradiate formation or for ventral PMC migration (Zuch et al., 2022). Thus, the sequence of events appears to be: 1. VEGF from VL ectoderm organizes PMC clusters and induces triradiate spicule formation before 18 hpf; 2. SLC/SPGs from VM (and VL)

ectoderm induces ventral PMC migration between 14 and 18 hpf; 3. LOX activity from VM ectoderm induces ventral biomineralization between 18 and 24 hpf (Fig. 3).

Here, we propose a novel approach to reproduce sea urchin larval skeletogenesis *de novo* by joining these different processes together using engineering tactics in a synthetic biology approach. We have developed a detailed protocol that will generate synthetic ectodermal cells with the previously described VL and VM gene expression profiles through microinjection, plate the dissociated cells on the extracellular matrix (ECM) with defined geometries along with generic ventral ectodermal cells to produce a monolayer lawn, then supply them with PMCs for *in vitro* skeletogenesis (Fig. 4A). In addition to being a tool for further exploration of skeletal mechanisms from a bottom-up perspective, this modular system opens the potential for biomedical applications. Synthetic calcium carbonate biominerals are of value in the STEM field for their superior tensile strength, high biocompatibility, and environmental-friendly production and disposal compared to calcium phosphate biominerals (Green et al., 2016; Zhao et al., 2019). Most of the existing approaches for generation of synthetic calcium carbonate biominerals either produce crude crystals that lack patterning or are limited to 2-dimensional biomineral films (Cavanaugh et al., 2019; Kim et al., 2011; Xiao et al., 2017). Our synthetic ectoderm culture, on the other hand, offers an exciting opportunity to engineer sophisticated, 3-dimensional calcium carbonate structures by shifting the focus from filling technical gaps in the engineering process to taking advantage of our knowledge of biological underpinnings of natural embryonic patterning systems and by

employing more widely available molecular methods, thus eventually encouraging the adaptation of our approach for a larger variety of synthetic purposes.

MATERIALS AND METHODS

Animals, gametes, and fertilization

L. variegatus sea urchins were obtained from Duke University Marine Lab (Beaufort, NC, USA) or Pelagic (Sugarloaf Key, FL, USA). Gametes were induced by intracoelomic injection of 0.5 M KCl. Eggs were washed three times with 50 mL of ASW and dejellied by gentle passage through 100- μ m Nitex mesh. Eggs were then fertilized with freshly diluted sperm (10 μ L concentrated sperm in 1.5 mL ASW) and washed twice with 50 mL ASW to remove excess sperm.

Preparation of hyalin

Hyalin extraction was performed as described (McClay and Fink, 1982; Robinson, 1988). Gametes of *L. variegatus* sea urchins were extracted as described above. Eggs were treated with 10 mM DTT for 5 minutes to disrupt the vitelline layer, then washed three times with ASW containing 10 mM Tris/HCl buffer, pH 8.0 and three times with ASW before fertilization and incubated at 23 °C for 2 hours. A suspension of embryos without fertilization membranes was incubated in HEM (hyaline extraction medium) with protease inhibitors (0.5 μ M Pefabloc and 0.5 μ g/mL Leupeptin) for 1-2 min. Embryos were pelleted by centrifuging at 600xg at 4°C for 20 seconds and supernatants were collected. The supernatant was then centrifuged 13,000 rpm on JA 25.50 at 4°C for 15 min to remove insoluble material. The pellet was discarded and hyalin was precipitated by addition of 20 mM CaCl₂ to the supernatant and centrifuged at 13,000 rpm for 30 min. The hyalin pellet was resuspended in 20 mL 2 mM EGTA, 10 mM Tris with protease inhibitors, precipitated with 20 mM CaCl₂, and centrifuged at 13,000 rpm at 4°C for 30

min twice more. The final pellet was homogenized and dialyzed against 2 mM EGTA, 10 mM Tris. The protein concentration was determined using BCA Protein Assay Kit (Pierce). For microcontact printing, purified hyalin were labeled with AlexaFluor 647 dye (Life Technologies) and stored in 10% glycerol at -80 °C. Hyalin gelation reactions were performed as described (Robinson, 1988).

Western blot

Western blot analysis of extracted hyalin was performed as described (Wessel et al., 1998). Positive control was prepared by centrifuging unfertilized eggs in HEM with 0.1% triton X-100 at top speed for 30 seconds and the supernatant was collected.

Microplate assay

A microplate assay was performed as described (Razinia et al., 2007). Briefly, 50 μ L of 12 hpf *L. variegatus* embryos (late blastula) were transferred into a 96-well polystyrene flat-bottom microplate. The embryos in each well were incubated at 23°C with 50 μ L of hyalin at a range of concentrations (0.00, 0.036, 0.075, 0.150 and 0.225 mg/mL) diluted in low calcium seawater, in triplicate. After an additional 12 hours, the embryos were photographed using DIC illumination with Zeiss Axio Imager A1 Upright Trinocular Fluorescence Microscope.

Gel electrophoresis and sequencing

The pCS2+ plasmid vector containing SpAxin (a gift from Dr. Athula Wikramanayake, University of Miami, FL, USA) and LvNodal cDNAs were linearized with NotI and mRNA was transcribed using the Ambion SP6 mMessage mMachine Kit (ThermoFisher Scientific). 1 μ L of RNA ladder (Ambion RNA Millennium Markers) and mRNAs were

treated with 10 μ L buffered formamide at 65 °C for 5 minutes, then run on 1% agarose gel. The predicted amino acid sequences of LvAxin (Echinobase, LOC446201) were compared with SpAxin (Echinobase, LOC576611) on Benchling (pairwise identity: 90%).

Microinjection

Gametes of *L. variegatus* sea urchins were extracted as described above. To eliminate fertilization envelopes, eggs were fertilized in 10 mM para-aminobenzoic acid (PABA) in ASW. The mRNAs were mixed with 20% glycerol to a final concentration of 1 μ g/ μ L and 0.35 μ g/ μ L for *LvNodal* and *SpAxin* mRNA, respectively, then loaded into microinjection needles. Zygotes were injected using standard methods as previously described (Bradham and McClay, 2006), transferred to a 24-well cell culture plate, and developed in ASW at 23°C. The experiments were repeated at least three times. The survival rates of mRNA injections were typically >90%. All mRNA-injected embryos were imaged using Zeiss Axio Imager A1 Upright Trinocular Fluorescence Microscope.

Immunostaining and confocal microscopy

Immunolabeling was performed as described (Bradham and McClay, 2006; Range et al., 2013). All images are full projections of z-stacks taken by Nikon C2+ confocal laser scanning microscope.

In situ hybridizations

Fluorescent *in situ* hybridizations were performed as described (Bradham et al., 2009). DIG-labeled antisense RNA probes were synthesized for the gene of interest using *in vitro* transcription (mMessage mMachine Kit, Ambion #Am1340) and purified with gel

exclusion chromatography using spin columns (Stratagene). Embryos rehydrated with PBST (phosphate-buffered saline with 0.1% Tween-20) were incubated with DIG-labeled probes overnight at 65°C in hybridization buffer (50% formamide, 5X SSC buffer, pH5, 50µg/mL yeast tRNA, 50µg/mL Heparin, 0.1% Tween 20). Embryos were washed in serial 2X – 0.1X SSCT dilutions at 65°C, then blocked with HISS/BSA (2% heat-inactivated sheep serum plus 5 mg/mL bovine serum albumin in PBST) at room temperature for 2 hours or overnight at 4°C, and finally incubated with anti-DIG conjugated to HRP (horseradish peroxidase, Perkin Elmer) in HISS/BSA for 30 min at room temperature. After washes with PBST, signals were developed for 6 min with Tyramide Signal Amplification Kit (Perkin-Elmer). Whole-mount *in situ* hybridizations were performed as described previously (Duloquin et al., 2007). All images are full projections of z-stacks taken by Nikon C2+ confocal laser scanning microscope.

Cell adhesion assay

Gametes of *L. variegatus* sea urchins were combined for fertilization as described above. 3-hour-old embryos (60-cell stage) were dissociated using methods modified from McClay and Marchase, 1979. Briefly, embryos were suspended in calcium-free ASW, triturated vigorously with P1000 micropipette tips, then P200 tips for 1 min total, washed and resuspended. Dissociated cells were labeled with SYTOX dead cell stain for examination of cell viability and Tetramethylrhodamine, methyl ester (TMRM) as a positive (mitochondrial) label before plating. Procedures for cell binding assay were modified from Fink and McClay, 1985. Briefly, aggregated hyalin proteins were either adsorbed onto the bottom of MatTek glass bottom dishes through overnight incubation or

seeded via microcontact printing. Aliquots of dissociated and labeled cells were then added to each dish and gently centrifuged into contact with the substrates. After washing, cell adhesion was examined under Nikon C2+ confocal laser scanning microscope.

RESULTS

Selection of Structural Components

To establish a functional synthetic ectoderm culture, both molecular and cellular requirements were considered. The cellular basis of ectoderm signaling to PMCs already dictates the two key components of this culture: ectodermal cells and PMCs, which can be generated through microinjection of mRNAs into zygotes. On the other hand, a specific molecular environment needs to be recreated to promote cell viability and motility. From that perspective, we consulted literature on the cellular environment of PMC migration and identified candidate components, described below, for the culture.

The diverse compositions of ECM on the apical and basal surface of the epithelium mediate differential cell adherence. To accurately recapitulate *in vivo* conditions for PMC migration, we aimed to establish the apical and basal compartments in the synthetic ectoderm culture using ECM proteins that are unique to each layer. Upon completion of ingress, PMCs lose their affinity for the apical hyaline layer (HA) and enter the blastocoel through holes in the basal lamina, containing mainly laminin along with collagen, which they stay attached to and migrate on during skeletal formation (Fink and McClay, 1985; Hertzler and McClay, 1999; Lyons et al., 2011). Due to its known role in PMC migration and convenient access as a commercial product, we decided to use laminin for basal recognition. We chose hyalin protein for the apical compartment, which is the major component of HA in sea urchins (McClay and Fink, 1982). Sequestered in cortical granules prior to fertilization, hyalin aggregates on the apical cell surfaces, oriented toward the exterior of the embryo, during and after cleavage stages (Lyons et al.,

2011; McClay and Fink, 1982). We extracted hyalin proteins following previously described methods (McClay and Fink, 1982; Robinson, 1988) and analyzed them using western blot. While the smears on the gel suggested the possibilities of either differential glycosylation or heterogenous lengths of hyalin proteins that corresponded to earlier discoveries, the highest molecular weight band of our extracted proteins is 230 kDa (Fig. 5A), which is far from the 330 kDa documented in previous literature (Wessel et al., 1998). This molecular weight, however, matched with echinonectin, another protein that is also unique to the apical ECM (Alliegro et al., 1988). To further evaluate the identity of our protein, we performed a microplate assay as described (Razinia et al., 2007). We found that embryos at mesenchyme blastula stage incubated with a low concentration of hyalin resulted in the abnormal phenotype of unattached archenterons at 24 hpf (Fig. 5C), which was consistent with the previously reported effect (Razinia et al., 2007). Assays that are more specific will need to be executed to verify the identity of extracted protein. For example, we can perform tryptic digestion and gelation reactions on these proteins (Robinson, 1988), then deduce its physical properties based on their bands. Hyalin proteins will form aggregates in certain concentrations of calcium and magnesium ions, resulting in higher molecular weight than 330 kDa (Robinson, 1988). Echinonectin, on the other hand, is a 230 kDa dimer and will dissociate into 116 kDa subunits in reducing conditions (Alliegro et al., 1988).

Upon reliable validation, the apical proteins will be labeled with Alexa Fluor 647 dye and either absorbed onto or stamped on MatTek glass bottom dishes in squares (Fig. 5D) via microcontact printing by Dr. Jeroen Eyckmans (Boston University, MA, USA)

for ectoderm cell adhesion assays. Previous studies and our preliminary observation (data not shown) have found that dissociated cells display preferential binding to plastic substrate (Roberson and Oppenheimer, 1975; Wu et al., 2011); therefore, surfaces without hyalin coating were treated with fetal bovine serum (FBS) to discourage cell adhesion.

Combining the two cell types, ectoderm and PMCs, and the apical and basal ECM proteins, we proposed the following assemblage for establishing a synthetic ectoderm culture. We planned to plate ectodermal cells between hyalin protein extracted from sea urchin embryos and commercial laminin protein, which will orient and maintain their polarity while providing structural support to the ectoderm and a substrate for PMCs during their migration to form skeletons (Fig. 4A). However, it is possible that exogenous hyalin is not sufficient to attract and bind ectodermal cells *in vitro* despite showing the affinity to orient them. In that case, we instead plan to use a transwell apparatus (Fig. 4B) as an alternative approach to the “sandwich” system shown in Fig. 4A. The ectoderm cells will be plated in the upper chamber, separated from PMCs in the lower chamber by a permeable membrane, which contains pores that prevent free passage of PMCs but are large enough for the protrusion of their filopodia to reach the ectoderm (Fig. 4B). The membrane will be coated with laminin on the side facing ectodermal cells to attach them, thus bypassing their potential lack of avidity with hyalin. Such arrangements will also ensure proper detection of the ectodermal patterning information by PMCs while keeping these cells in distinct compartments.

Microinjection and Identification

In general, we planned to establish two cell identities, PMCs and ectoderm, through microinjection of specific mRNAs into embryos at fertilization (Fig. 6). We will produce PMCs by injecting *pmar1* mRNA, since Pmar1 expression is sufficient to specify every cell in the embryo as a PMC (Oliveri et al., 2002; Oliveri et al., 2003) (Fig. 6, red). We will generate generic ventral ectodermal cells by co-expressing Axin (an inhibitor of cWnt pathway) and Nodal, the inducer of ventral identity (Sun et al., 2021; Duboc et al., 2004). Axin-mediated cWnt inhibition results in ectopic expression of the anterior neuroectoderm (ANE) identity throughout the embryo (Range et al., 2013; Sun et al., 2021), consistent with the previous findings that nuclearization of β -catenin is required both for endomesoderm specification and to suppress a global neural fate (Logan et al., 1999; Yaguchi et al., 2006). Addition of Nodal expression will simultaneously specify the ventral identity, leading to establishment of ventral ectoderm, and suppress the neural ectodermal fate (Duboc et al., 2004; Yaguchi et al., 2007). To produce the VL ectoderm identity that will pattern skeletal triadiates, we will co-inject *vegf* mRNA along with Axin and Nodal (Fig. 6, cyan). To generate VM ectoderm, we will instead co-inject *slc* and *lox* mRNAs (Fig. 6, purple). To distinguish these different types of cells in the culture, mRNAs encoding the following fluorescent markers will be co-injected: mCherry for PMCs, EGFP for VL ectoderm, and cerulean-tagged histone 2B for VM ectoderm (Fig. 6).

In preparation for microinjection for ventral ectoderm, *SpAxin* (*Strongylocentrotus purpuratus Axin*) and *LvNodal* (*Lytechinus variegatus Nodal*) mRNAs were synthesized and inspected using gel electrophoresis, where they appeared

as 3.5 kilobases (kb) and 1.5 kb bands, respectively (Fig. 7A), consistent with their expected sizes. High pairwise identity between amino acid sequences of SpAxin and LvAxin from protein analysis (Fig. 7B) indicated that our *SpAxin* mRNA should be sufficient to replicate Axin phenotypes in *L. variegatus*.

For PMCs, overexpression of *LvPmar1* mRNA converted the embryos into piles of mesenchyme cells at 12 hpf (Fig. 8C1), as expected (Fig. 8C2). Injection of *SpAxin* and *LvNodal* mRNA resulted in expected morphologies, matching previously established phenotypes from earlier studies. Exogenous Axin gave the embryo a round appearance with clear blastocoel and thickened ectoderm with abundant cilia (Fig. 8D1); this phenotype is known as a dauer blastula and reflects the absence of endomesoderm (Sun et al., 2021) (Fig. 8D2). Overexpression of Nodal resulted in embryos with regular gut formation, ectopically positioned ciliary bands, and a radialized, posterior skeleton that lacked arm extensions (Fig. 8E1), consistent with the expected outcomes (Duboc et al., 2004; Bradham et al., 2009) (Fig. 8E2). Combining the traits from both injections, we expect the co-injected embryos to exhibit the elongated AP axis, to lack an archenteron due to inhibition of endomesoderm specification, and to be uniformly specified as ventral ectoderm.

In addition to morphology corroboration, to verify successful conversion of cell identities by microinjection, we will carry out a series of molecular characterization on injected embryos. Inhibition of the cWnt pathway promotes an expansion of ANE (Logan et al., 1999; Range et al., 2013; Range, 2018; Sun et al., 2021) where serotonergic neurons are located (Range and Wei, 2016). Hence, for embryos injected with *SpAxin*

mRNA, we will check for amplification of neural signals using antibodies against serotonin (ser, Fig. 9A). Effective injection of *LvNodal* mRNA will be confirmed with immunofluorescence against ser, synaptotagmin B (synB), and primary antibody 295 for ciliary bands. Nodal overexpression repositions synB neurons and the ciliary band to the posterior while suppressing serotonergic neuron specification (Fig. 9B-C), in keeping with an expansion of the ventral ectodermal fate (Bradham et al., 2009). We will assess the co-injected embryos with both immunostaining and WMISH for marker gene expression. Nodal expression should counteract the pro-neural effects of Axin expression and eliminate all serotonergic neuron signals; this combination will probably also eliminate or strongly reduce synB and ciliary band specification, since both AV and DV specification will be perturbed. For combined overexpression of Nodal and Axin, we anticipate observing elevated levels of *Chordin* (*Chd*) and *Gooseoid* (*Gsc*), which are both downstream from Nodal and act to specify ventral ectoderm (Fig. 9D), and a loss of endomesoderm markers due to Axin-mediated cWnt inhibition, including PMC markers such as *Tbrain*, *Alx1*, and endomesoderm markers such as *Pks1* and *GataE* (Angerer et al., 2001; Bradham and McClay, 2006; Bradham et al., 2009; Lyons et al., 2011; Yuh et al., 2004).

Cell Adhesion Assay

To test the competency of hyalin to adhere to ectodermal cells, we will perform a cell adhesion assay. Injected embryos used to supply synthetic ectoderm cells will be dissociated when they develop to the 60-cell stage, at which point the cell fates have been specified (Lyons et al., 2011). We will plate the disaggregated cells onto hyalin printed

substrate as described previously (Fig. 5D) then centrifuge them lightly to promote their attachment (Fig. 10A). After loosely or unattached cells are washed out, cell adhesion will be examined using confocal microscopy, which allows for simultaneous detection of Alexa-647-labeled hyalin and various fluorescent signals from the dissociated ectodermal cells (see Fig. 6). During our trial experiments using control embryos at the 60-cell stage, disaggregated cells displayed single cell suspension (Fig. 10B1) and high cell survival as indicated by negligible detection of SYTOX dead cell stain (Fig. 10B2). However, cells did not adhere to hyalin as expected, which could be explained by a previous discovery that cells of different lineages showed differential affinity for hyalin and that cell-cell association overrode cell-hyaline interactions later in development (McClay and Fink, 1982). Therefore, the adhesion assay needs to be repeated with microinjection-generated ectodermal cells only. If ectodermal cells adhere to hyalin, then we will assemble the synthetic ectoderm as depicted in Fig. 4A, using printed hyalin substrates.

Assemblage and Further Modification

Upon satisfactory assessment of the ability of hyalin to mobilize and bind ectodermal cells, we will assemble the synthetic ectoderm culture with the apical compartment serving as the base of the culture (Fig. 4A). However, if hyalin is insufficient for ectodermal adhesion, we will instead assemble the culture in a transwell system, plating ectodermal cells on laminin (Fig. 4B). In that case, we will first coat the permeable membrane with laminin, then flip the upper chamber and seed PMCs on the reverse side of the membrane. After PMCs have stably attached to the laminin, we will invert the chamber back in original orientation and plate ectodermal cells in the upper

chamber on top of the laminin. To finish, we will position hyalin on the ectodermal cells for apical recognition. We will also test plating the ectodermal cells first, inverting the adhered ectoderm, then subsequently adding PMCs.

After successfully creating the “sandwich” ectodermal cultures described above, we plan to enhance the complexity of the ectoderm by adhering the VL and VM ectodermal cells in defined geometries via cell culture inserts (Fig. 11). These silicone inserts come in different sizes and shapes, and can be custom-made, to allow for positioning confined patches of VL or VM ectoderm cells on the laminin-coated membrane (or hyaline-coated surface). After removing the silicone insert, we will cover the rest of the surface with ventral ectodermal cells. We predict that when VL ectoderm is added as islands among generic ventral ectodermal cells, PMCs will migrate to VL ectoderm patches, then secrete skeletal triradiates in response to the local VEGF signals (Fig. 11A). If VM ectoderm is seeded in a similar fashion, the SPG and LOX signals will attract PMCs to form single-cell chains instead of clusters, and subsequently secrete spicules in the shape of linear rods (Fig. 11B). When VL and VM ectoderm are each achieved successfully, we will add VM ectoderm to bridge two islands of VL ectoderm, with the prediction that PMCs will form two clusters on the VL ectoderm joined by a chain of PMCs on the VM ectoderm. We further predict that this collection of PMCs together will secrete interconnected skeletons in which two lateral triradiates, induced by VEGF signals from the VL ectoderm, are connected by an intervening linear spicule that corresponds to a VT, induced by SPG and LOX in the VM ectoderm (Fig. 11C).

DISCUSSION

Calcium carbonate biomineral production is under extensive investigation as a highly preferred material for industrial and research applications. Here, we proposed a synthetic ectoderm culture system to generate calcite biominerals by taking advantage of the natural skeletal patterning process in *L. variegatus* sea urchins. Previous studies have revealed the principles underlying this biological process in which ectodermal cues instruct adjacent PMCs to migrate and secrete spicules during skeletal patterning. We therefore hypothesized that, if we generate specific types of ectodermal cells via microinjection of genes that are endogenously expressed in distinct ectodermal locations and spatially organize those cells, they can signal to PMCs to form corresponding patterned skeletons *in vitro*.

So far, we have extracted ECM protein hyalin and performed microplate assays to verify their exogenous effect on sea urchin gastrulation. We have also labeled and patterned our hyalin on plastic substrates via microcontact printing. To examine the interaction between hyalin and ectodermal cells, we have dissociated embryos at 60-cell stage into single cells and plated them on hyalin-coated substrates. Results from these adhesion assays, however, have shown that these cells indistinguishably bind to hyalin as well as uncoated areas of the substrate. When we treated uncoated surfaces with FBS to discourage cell adhesion, cells exhibited even less adherence to the hyalin-coated areas. Previous literature has found that cells of heterogenous germ layers preferred to aggregate among themselves than with hyalin (McClay and Fink, 1982). Hence, we speculated that these dissociated cells from control embryos, featuring all three

presumptive germ layers, aggregated among themselves instead of attaching to hyalin. To address this problem, we moved on to synthesize selective ectodermal cells for dissociation through microinjection.

In terms of generating ectodermal cells, we have synthesized *SpAxin* and *LvNodal* mRNAs, each showing bands at expected sizes upon agarose gel electrophoresis. Injections of these mRNAs have yielded phenotypes that are comparable to those established in previous literature. We consulted the Sun et al., 2021 report that used the same *SpAxin* mRNA construct for optimal injection concentrations; however, embryos from the initial attempts of injection either differed from published morphologies or lacked uniformity despite receiving the same dosage of mRNA. To discern the cause, we first examined the mRNA on gel to check for potential RNA degradation in the stock solution. In cases where degradation was observed as smears on the gel, we carried out a series of measures to control for RNase contamination including treating water used for dissolving mRNAs with diethyl pyrocarbonate (DEPC) to inactivate RNase, using 70% ethanol to sanitize working areas, wearing and changing personal protective equipment frequently, and avoiding contact with reagents and injection needles as much as possible. We also tackled technical deficiencies such as incomplete dissolution of mRNAs by thoroughly mixing the solution with a micropipette before use.

One challenge that we envisage with dissociating cells from microinjection concerns limited quantity. This was not a problem in the dissociation trials, because we were able to fertilize and dissociate all the eggs collected from female urchins, which can produce millions of gametes in one spawn (Lyons et al., 2011). For one plate of

microinjection, however, eggs are lined in a single row in a 60-mm culture dish (see Fig. 8A), which equals around 100-200 eggs. Additionally, all eggs need to be fertilized at the same time to reach the 60-cell stage together for dissociation, then injected in approximately one hour before the first cell division. Under one hour, four plates at maximum can be injected, yielding less than 800 embryos for one dissociation event. One potential solution to this problem is to decrease the surface area of substrates by using terasaki plates, whose individual well holds a volume of 10 μ L. This way, we will be able to concentrate the dissociated cells and still have sufficient volume to form a monolayer in each well for cell adhesion assay. Nevertheless, low yield remains a challenge for transwell assemblage in later experiments, in which cases we will consider manipulating gene expression through transfection via lentivirus in place of microinjection for increasing cell production.

Moving forward, we will test the sufficiency of co-expressing Nodal, Axin, and VEGF in creating functional VL ectoderm. Specifically, we will assess the ability of these cells to attract PMCs as clusters, whose fluorescence will be visible under confocal microscopy, and to instruct PMCs to generate triradiates, the birefringent appearance of which will be straight forward to capture under plane-polarized light, as exemplified in Fig. 1B3. We will also carry out FISH in PMCs to detect signals of Jun, which is downstream from VEGF and endogenously expressed in VLCs (Zuch et al., 2022); Jun is therefore predicted to be expressed by PMCs that are adjacent to and receive patterning instructions from VL ectoderm in our synthetic system. If VEGF alone is not sufficient for these three effects, we will successively include Wnt5, SLC, and LOX expression in

these ectodermal cells to reinforce their VL identity (McIntyre et al., 2013; Piacentino et al., 2016; Zuch et al., 2022).

Similarly, we will test whether the combination of LOX and SLC with Nodal and Axin can successfully establish the VM ectoderm by examining their ability to attract a single chain of PMCs, to instruct PMCs to produce linear skeletal rudiments when plated in defined stripes (via silicon inserts) amid ventral ectoderm, and to induce the expression of Polyketide-synthase 2 (Pks2) in PMCs, which is known to be exclusively expressed in medial region of ventral PMCs (Sun and Etensohn, 2014; Zuch et al., 2022). If these effects are not induced, we will further posteriorize the ectoderm by adding the expression of the Eve transcription factor (Li et al., 2014). If successful, we will proceed to combine the two ectodermal types, flanking VM ectoderm with VL ectoderm, among ventral ectodermal cells (Fig. 11C). Here, we anticipate that this system will induce the formation of triradiates connected by linear spicules.

Our investigation into synthesizing calcium carbonate biominerals foresees many technical and adaptive challenges, especially as we proceed to more advanced stages. It is nonetheless still highly feasible with mature protocols and technologies and abundant literature available for consultation. Moreover, the completion of this project will provide the initial proof of concept for a biological system that generates customized calcium carbonate biominerals. In addition to sea urchins, usage of transformed ACC for biomineralization has been observed in many other species such as marine bivalves *Mercenaria mercenaria* and *Crassostrea gigas*, naces, earthworms, and crustaceans (Beniash et al., 1997; Weiss et al., 2002; Nassif et al., 2005; Hodson et al., 2015; Neues

et al., 2007). ACC can be used to further synthesize hydroxyapatite, which is the key building block of human bone and is used widely in bone regeneration (Smotrina et al., 2019; Sawada et al., 2021). Henceforth, further understanding of biomineral production in sea urchins is highly valuable across a range of engineering and biomedical applications. The work in this thesis has contributed to those first steps to establish proof of concept for this synthetic biology approach.

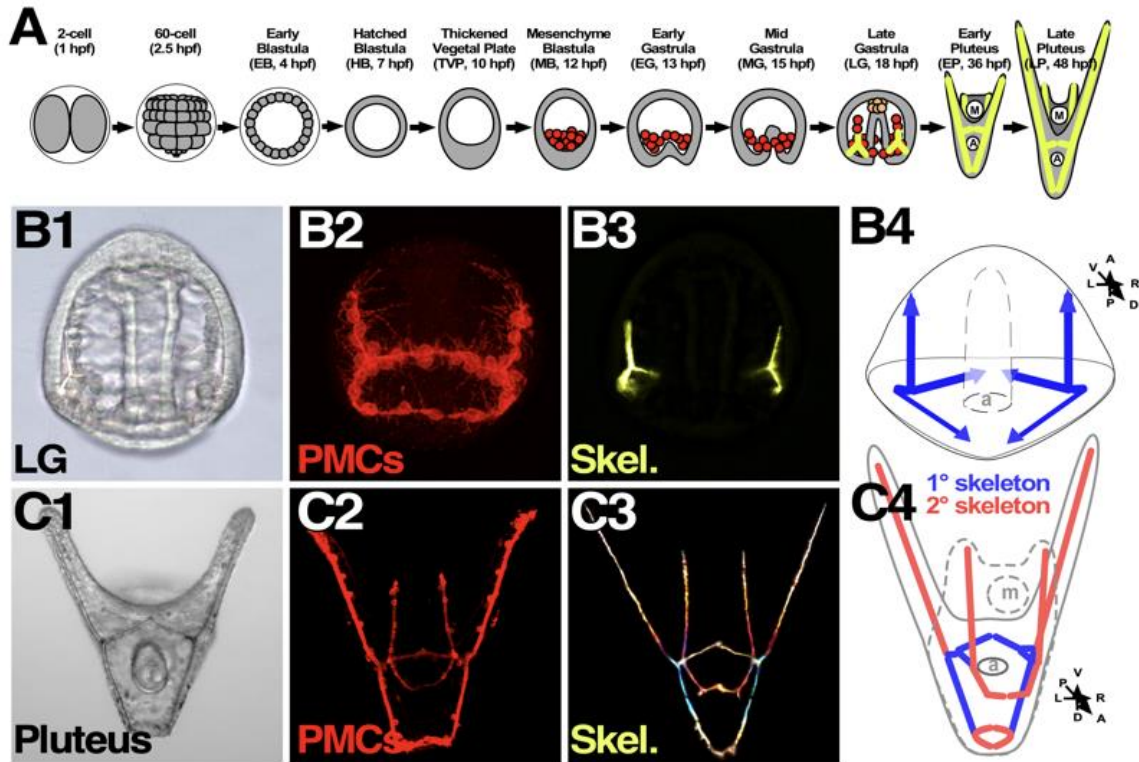


Figure 1. PMCs secrete the larval skeleton in 1° and 2° patterning stages after gastrulation. A. A schematic of the first 48 hours of development of *L. variegatus* that shows PMCs (red) and skeleton (yellow); mouth (m) and anus (a) are indicated. The timing of each stage is indicated as hours post-fertilization (hpf). **B.** At late gastrula stage (B1), PMCs migrate to a ring-and-cord primary (1°) pattern (B2) and initiate the skeleton as bilateral triradiates (B3) within the ventrolateral PMC clusters. The ring-and-cords pattern corresponds with the subsequent biomineral structures that produce the major ventral, dorsal, and anterior-posterior elements (B4). **C.** To form the pluteus larva (C1), PMCs migrate away from the 1° pattern to produce the long posterior rods and the anterior elements (C2, C3) that correspond to the secondary (2°) skeleton (C4, red). Control embryos are shown with differential interference contrast illumination (DIC, 1),

PMC-specific immunostaining (2), birefringence of the calcium carbonate skeleton (via illumination with plane-polarized light, 3), and schematics indicating 1° (blue) and 2° (red) skeletons (4) in the corresponding stages. A. adapted from (Hogan et al., 2020); B.-C. adapted from (Zuch and Bradham, 2019).

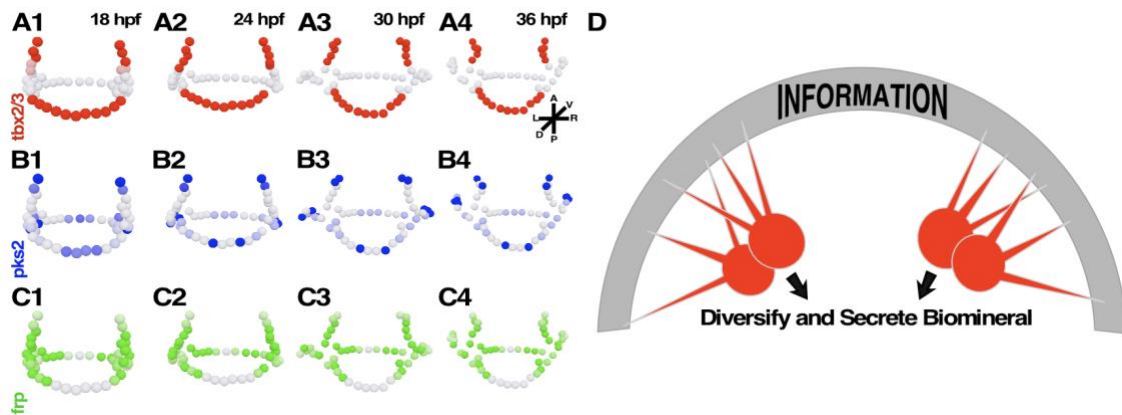


Figure 2. PMCs diversify their gene expression profiles during skeletal patterning.

A.-C. Models of averaged FISH data in *L. variegatus* embryos for *tbx2/3* (A), *pks2* (B) and *frp* (C) are shown at the indicated time points during 1° (1) and 2° (2-4) patterning.

D. The schematic shows the current model for the interactions between PMCs (red) and ectoderm cells (gray) during skeletal patterning. PMCs extend filopodia to ectodermal cells presumably to receive signals, upon which the PMCs diversify, then secrete skeletal spicules. A.-C. adapted from (Zuch and Bradham, 2019).

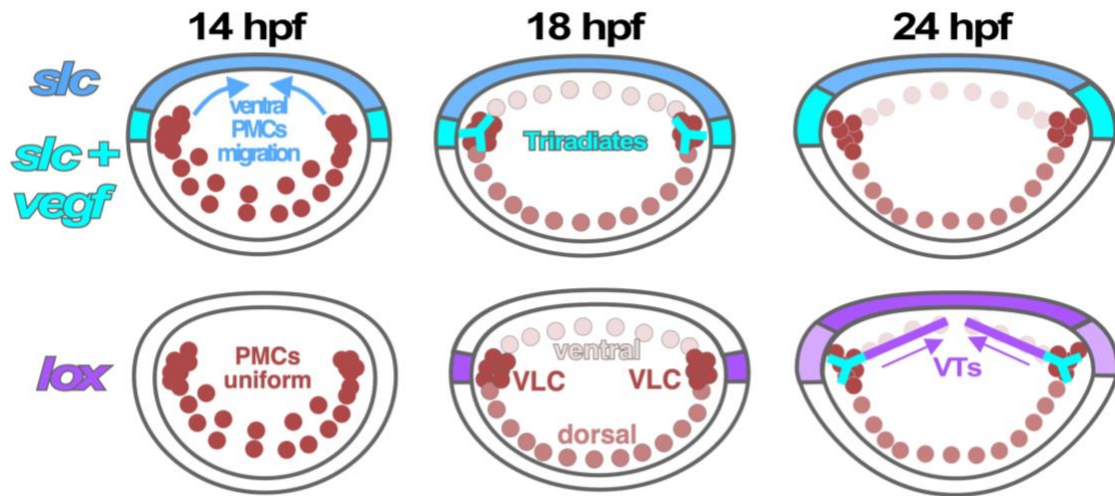


Figure 3. A model for early skeletal patterning. The schematics depict the posterior PMCs at the indicated time points, with the ectodermal spatial expression domains of *slc* (blue), *vegf* (cyan), and *lox* (purple) shown, along with PMC dynamics. Vegf is necessary and sufficient for PMC cluster formation and triradiate formation, which occurs between 14 and 18 hpf. Slc is required for ventral PMC migration between 14-18 hpf, but not for triradiate formation. Finally, *lox* is required for VT biomineralization between 18-24 hpf, but not for ventral PMC migration or triradiate formation.

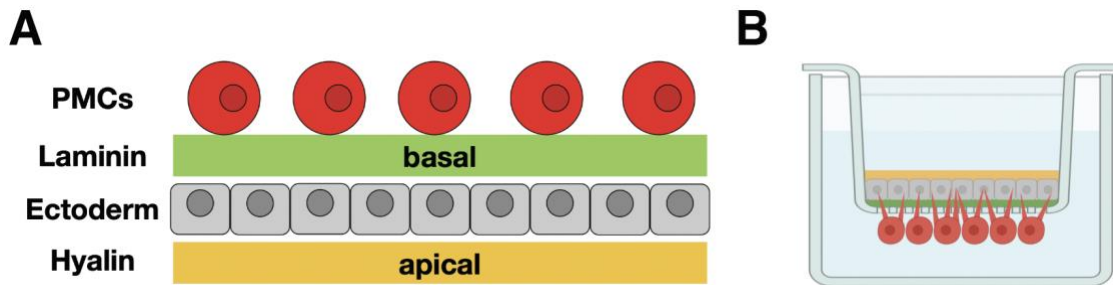


Figure 4. The proposed synthetic ectoderm and PMC culture approach. A.

“Sandwich” system. Ectodermal cells (gray) are positioned between ECM layers of hyalin proteins (yellow) representing the apical compartment and laminin (green) representing the basal compartment, upon which PMCs (red) are positioned. **B.**

Transwell model. If hyalin is insufficient to attach ectodermal cells, this assembly will be flipped to for use in transwells where the laminin (green) is coated on the permeable membrane in the upper chamber while PMCs are seeded on the reverse side of the membrane in the lower chamber.

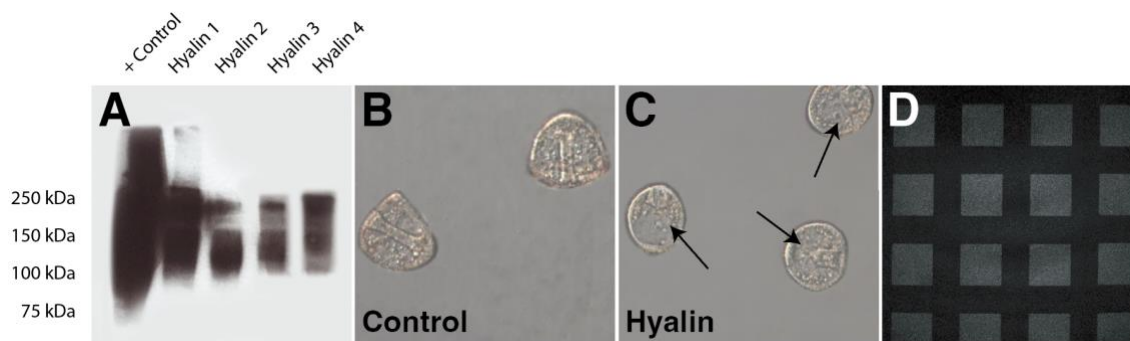


Figure 5. Evaluation and stamping of hyalin protein. **A.** Western blot analysis of four separate hyalin extractions all displayed bands at 230 kDa. Lysates of unfertilized eggs containing hyalin proteins were used as positive (+) control. **B.-C.** Microplate assay was conducted by treating *L. variegatus* embryos at mesenchyme blastula stage with 0.036-0.075 mg/mL of the hyalin preparation diluted in ASW. Control embryos imaged at 24 hpf have full-length archenteron (**B**) while hyalin-treated embryos exhibited incomplete archenteron elongation (**C**, arrows). **D.** Hyalin protein labeled with Alexa 647 (50 $\mu\text{g}/\text{mL}$) was patterned into squares on glass by microcontact printing followed by fluorescence imaging.

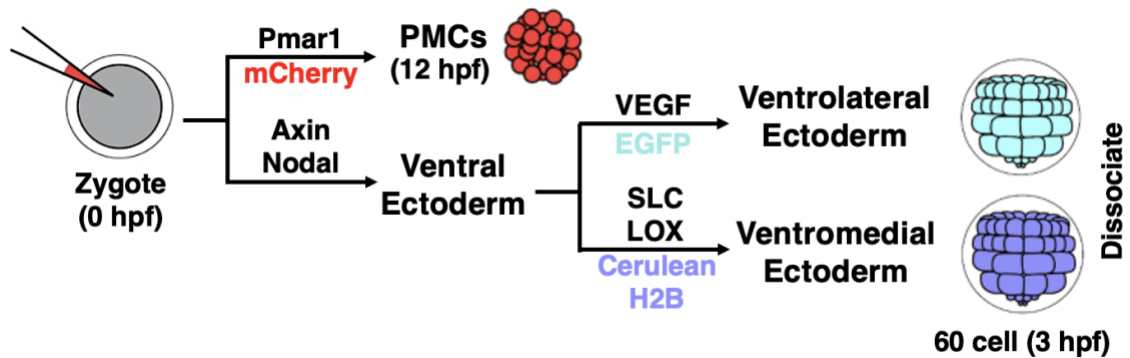


Figure 6. The proposed workflow to generate the cell types for the synthetic system.

The schematic depicts the genes that will be overexpressed to generate PMCs (red) and specific subtypes of ectoderm cells (cyan and purple), along with fluorescent markers for each type. For PMC preparation, overexpression of *Pmar1* mRNA will render all cells mesenchymal PMCs at 12 hpf. For ectoderm preparations, zygotes will be injected with indicated mRNAs, then dissociated at the 60-cell stage.

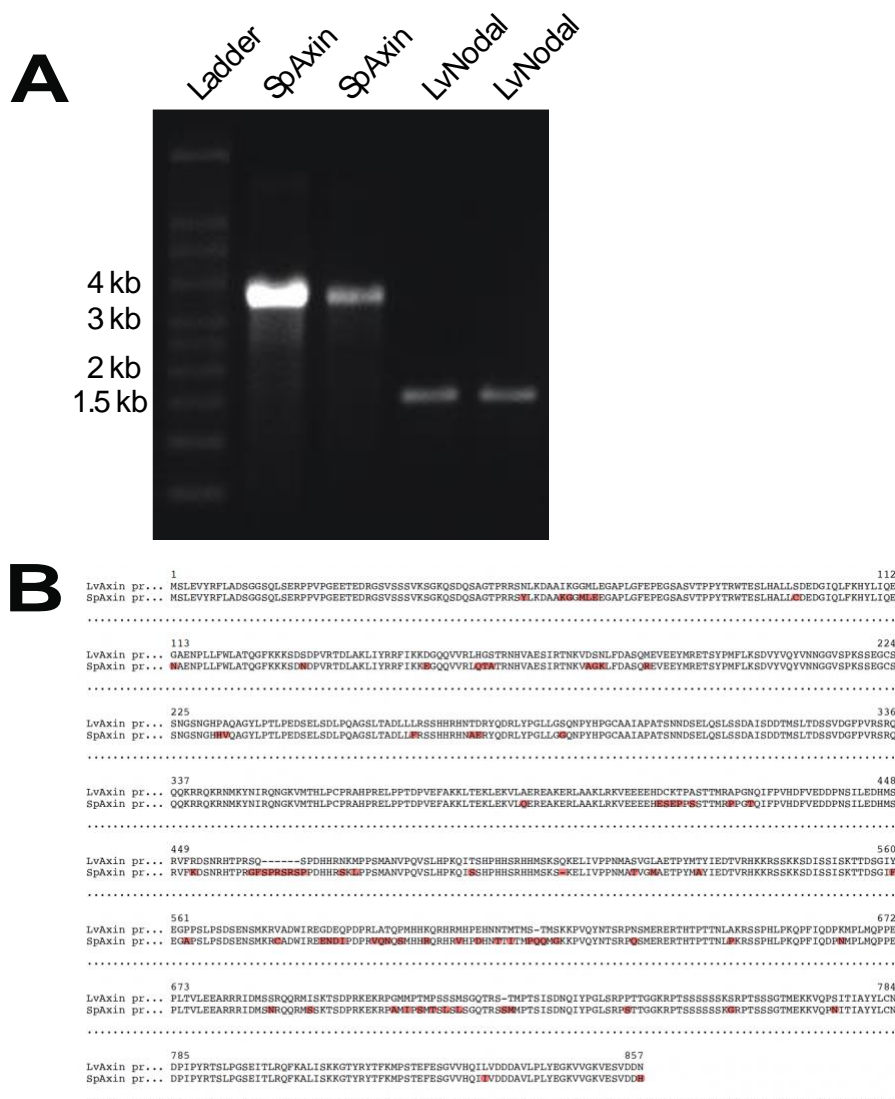


Figure 7. Preparation of Axin and Nodal mRNAs for microinjection. A. Agarose gel electrophoresis shows that each indicated *in vitro*-transcribed mRNA migrates at the expected size, with minimal degradation. B. Echinoderm Axin protein sequence alignments show 90% identity between Lv and SpAxin.

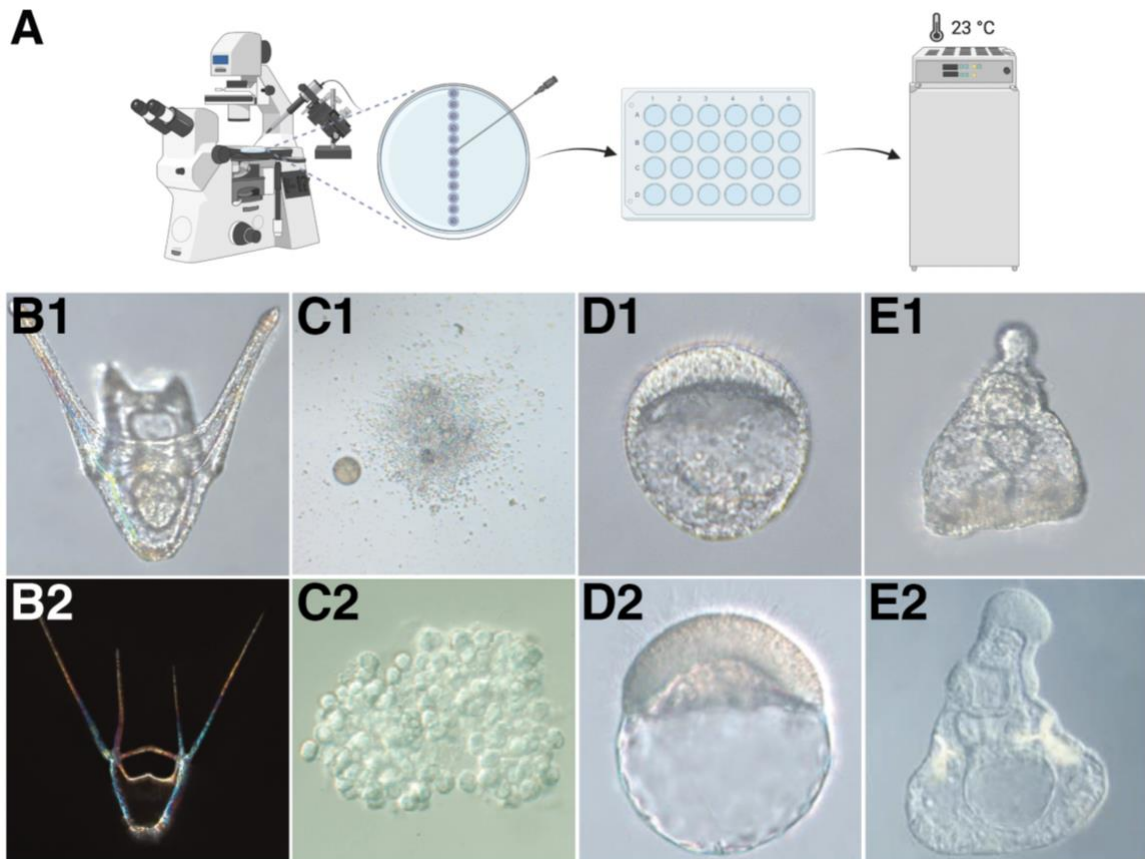


Figure 8. Gene overexpression produces the expected phenotypes. A. The process of microinjection is shown schematically. **B.** Live DIC image (B1) and skeletal birefringence in the same embryos (B2) of a control 48-hour pluteus larva. **C.** *L. variegatus* embryos were injected with *Pmar1* mRNA, then imaged by (DIC) at 18 hpf (C1). Injected embryos were transformed to uniform mesenchymal cells; an uninjected egg is also shown for contrast (C1). This phenotype matches well with previously published results from *Paracentrotus lividus* embryos at 72 hpf (C2, adapted from Duloquin et al., 2007). **D.** An *L. variegatus* embryo injected with *SpAxin* mRNA is shown at 48 hpf (D1). Overexpression of Axin anteriorized the embryos and inhibited gastrulation; this phenotype is very similar to the expected phenotype, shown at 72 hpf

(D2, adapted from Sun et al., 2021). **E.** An *L. variegatus* embryo injected with *LvNodal* mRNA is shown at 48 hpf (E1). Overexpression of *Nodal* radialized the embryos and induced formation of bell caps at the animal pole; this phenotype matches the previously published phenotype in *P. lividus* at 72 hpf (E2, adapted from Duboc et al., 2004).

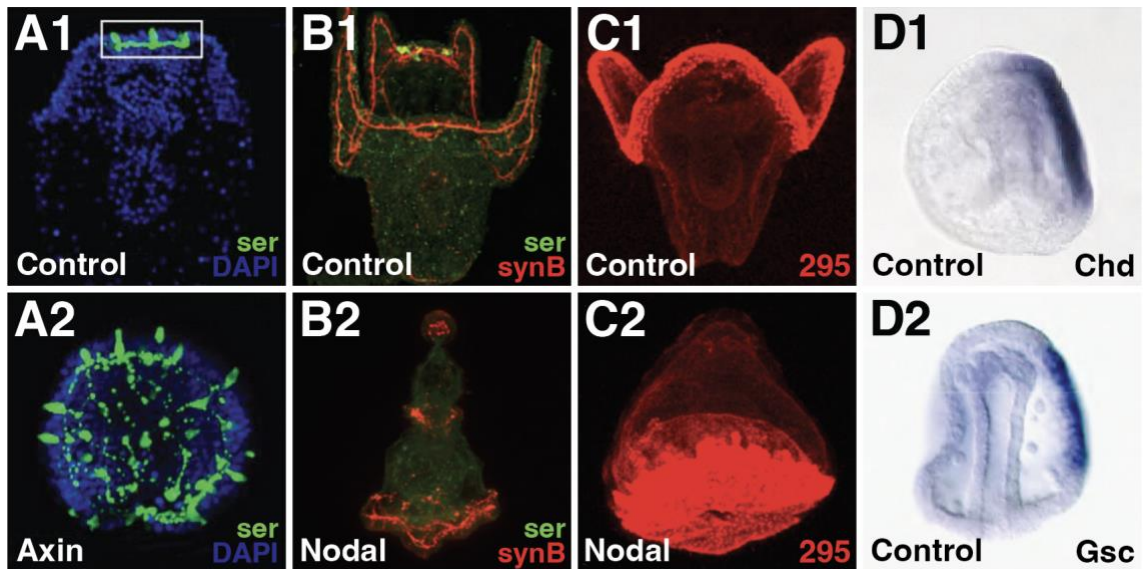


Figure 9. The proposed strategy to confirm cell identities using established molecular markers of ectoderm cell types. A. Neural cells were labeled with antibodies against serotonergic neurons (green) and nuclei (blue) in 84 hpf *S. purpuratus* plutei control (1) and *Axin*-injected (2) embryos. White box outlines the ANE. **B.-C.** Serotonergic neurons (B, green), synaptotagmin-B (B, red) and ciliary band (C, red) labeled with monoclonal primary antibody 295 in 24-hour *L. variegatus* plutei control (1) and *Nodal*-injected (2) embryos. Embryos are imaged with confocal microscopy and shown as full projections of z-series in lateral views, oriented with the animal pole toward the top. **D.** WMISH quantification of LvChd (D1) and LvGsc (D2) expression in control embryos at late gastrula stage are shown in lateral views. A. adapted from (Range et al., 2013). B.-D. adapted from (Bradham et al., 2009).

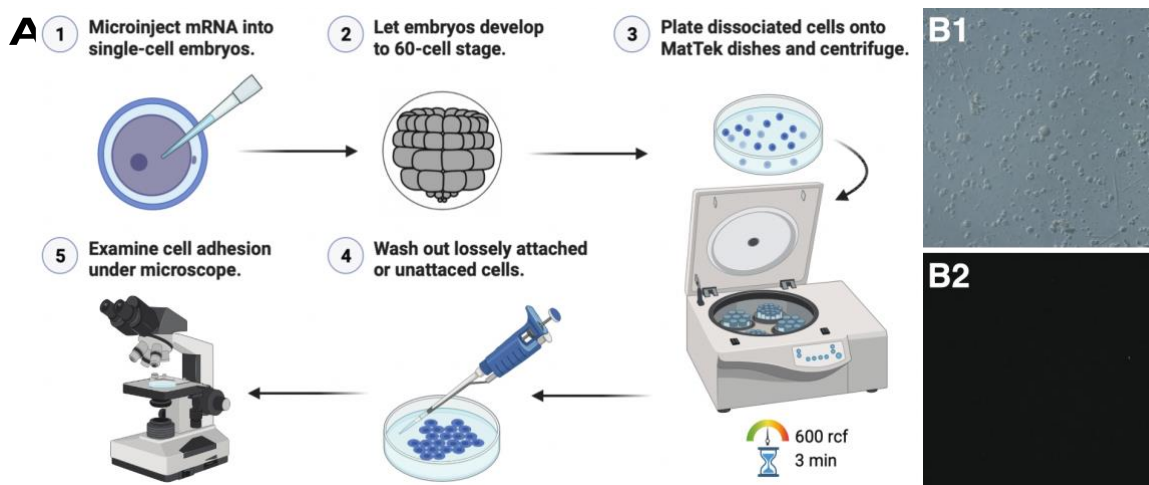


Figure 10. The proposed plating approach using disaggregated ectoderm cells and hyalin. A. The diagram shows the process of cell dissociation and plating, for preliminary experiments. Microinjected embryos are disaggregated at 60-cell stage and dispensed onto MatTek dishes stamped with hyalin protein. After a light centrifugation with plate carriers, dishes are washed with ASW to remove unattached cells, then examined under a microscope. **B.** The morphology (DIC, B1) and SYTOX dead cell stain (green, B2) of control embryos dissociated at 60-cell stage revealed single cell suspension and high cell viability, but low cell density.

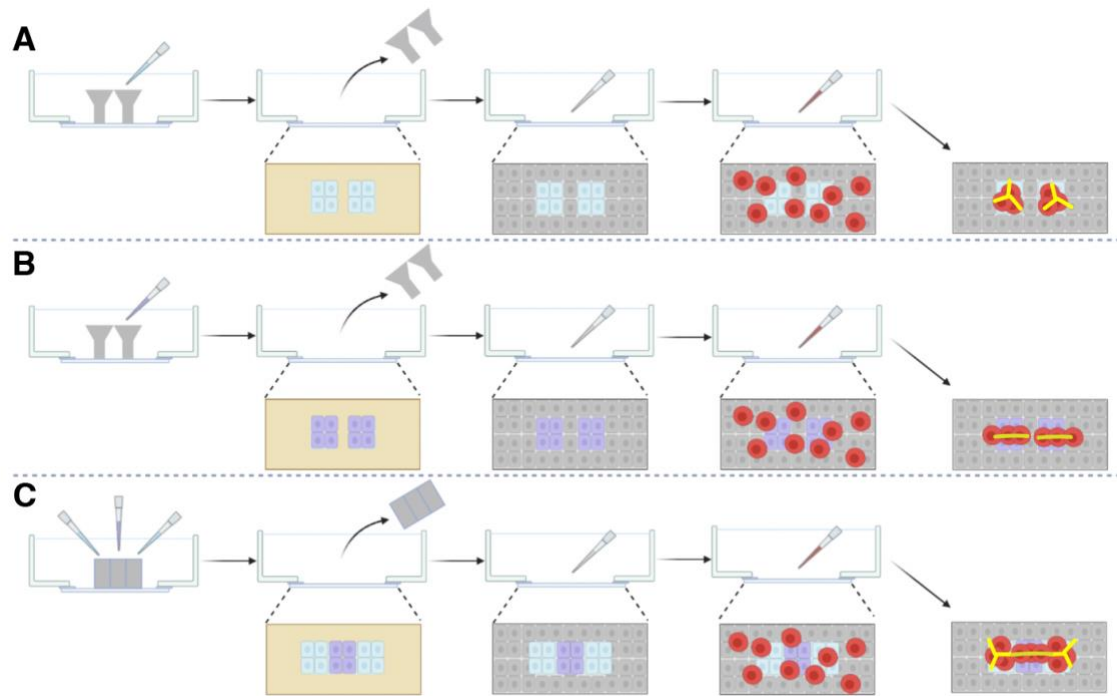


Figure 11. Proposed approach for the synthetic complex ectoderm culture. We will generate different types of ectoderm cells according to the cell injection workflow (Fig. 6), then spatially confine them using silicone culture inserts. **A.** We will confine VL ectoderm cells (cyan), then plate generally with ventral ectoderm cells (gray). We will then add PMCs (red) to this system, with the prediction that PMCs will occupy the VL ectodermal spots as clusters of cells, then secrete skeletal triradiates (yellow) in those locations. **B.** We will confine VM ectoderm cells (purple), then plate generally with ventral ectoderm cells (gray). We will then add PMCs (red) to this system, with the prediction that PMCs will occupy the VM ectodermal spots as chains of cells, then secrete rod skeletons (yellow) in those locations. **C.** Next, we will increase the complexity of the system by adding spots of VM ectoderm (purple) flanked by VL ectoderm (cyan), using a more complex silicon insert. We predict that the VM ectoderm

will promote the formation of linear elements that interconnect skeletal triradiate when positioned between VL ectoderm spots, similar to the *in vivo* arrangement.

BIBLIOGRAPHY

- Adomako-Ankomah, A., Ettensohn, C.A., 2013. "Growth factor-mediated mesodermal cell guidance and skeletogenesis during sea urchin gastrulation." *Development* 140: 4214-4225.
- Alliegro, M.C., Ettensohn C.A., Burdsal, C.A., Erickson, H.P., McClay, D.R., 1988. "Echinonectin: A New Embryonic Substrate Adhesion Protein." *The Journal of Cell Biology* 107 (6): 2319-327.
- Angerer, A.L., Angerer, R.C., 2000. "Animal-Vegetal Axis Patterning Mechanisms in the Early Sea Urchin Embryo." *Developmental Biology* 218 (1): 1-12.
- Angerer, L.M., Oleksyn, D.W., Levine, A.M., Li, X., Klein, W.H., Angerer, R.C., 2001. "Sea Urchin Goosecoid Function Links Fate Specification along the Animal-Vegetal and Oral-Aboral Embryonic Axes." *Development (Cambridge)* 128 (22): 4393-4404.
- Armstrong, N., Hardin, J., McClay, D.R., 1993. "Cell-cell Interactions Regulate Skeleton Formation in the Sea Urchin Embryo." *Development (Cambridge)* 119 (3): 833-840.
- Beniash, E., Addadi, L., Weiner, S., 1999. "Cellular Control Over Spicule Formation in Sea Urchin Embryos: A Structural Approach." *Journal of Structural Biology* 125 (1): 50-62.
- Beniash, E., Aizenberg, J., Addadi, L., Weiner, S., 1997. "Amorphous calcium carbonate transforms into calcite during sea urchin larval spicule growth." *Proceedings: Biological Sciences* 264 (1380): 461-465.
- Bradham, C.A., McClay, D.R., 2006. "P38 MAPK Is Essential for Secondary Axis Specification and Patterning in Sea Urchin Embryos." *Development (Cambridge)* 133 (1): 21-32.
- Bradham, C.A., Oikonomou, C., Kühn, A., Core, A.B., Modell, J.W., McClay, D.R., Poustka, A.J., 2009. "Chordin Is Required for Neural but Not Axial Development in Sea Urchin Embryos." *Developmental Biology* 328 (2): 221-233.
- Cavanaugh, J., Whittaker, M.L., Joester, D., 2019. "Crystallization kinetics of amorphous calcium carbonate in confinement." *Chemical Science (Cambridge)* 1 (19): 539-543.
- Duboc, V., Lapraz, F., Besnardeau, L., Lepage, T., 2008. "Lefty acts as an essential modulator of Nodal activity during sea urchin oral-aboral axis formation." *Developmental Biology* 320 (1): 49-59.

- Duboc, V., Röttinger, E., Besnardeau, L., Lepage, T., 2004. "Nodal and BMP2/4 Signaling Organizes the Oral-Aboral Axis of the Sea Urchin Embryo." *Developmental Cell* 6 (3): 397-410.
- Duloquin, L., Lhomond, G., Gache, C., 2007. "Localized VEGF Signaling from Ectoderm to Mesenchyme Cells Controls Morphogenesis of the Sea Urchin Embryo Skeleton." *Development (Cambridge)* 134 (12): 2293-2302.
- Ettensohn, C.A., 1990. "The Regulation of Primary Mesenchyme Cell Patterning." *Developmental Biology* 140 (2): 261-71.
- Fink, R.D., McClay, D.R., 1985. "Three Cell Recognition Changes Accompany the Ingression of Sea Urchin Primary Mesenchyme Cells." *Developmental Biology* 107 (1): 66-74.
- Green, D.W., Ben-Nissan, B., Yoon, K.S., Milthorpe, B., Jung, H., 2016. "Natural and Synthetic Coral Biomineralization for Human Bone Revitalization." *Trends in Biotechnology* 35 (1): 43-54.
- Hertzler, P.L., McClay, D.R., 1999. "αSU2, an epithelial integrin that binds laminin in the sea urchin embryo." *Developmental biology* 207: 1-13.
- Hodson, M.E., Benning, L.G., Demarchi, B., Penkman, K.E., Rodriguez-Blanco, J.D., Schofield, P.F., Versteegh, E.A., 2015. "Biomineralisation by earthworms - an investigation into the stability and distribution of amorphous calcium carbonate." *Geochemical Transactions* 16: 4.
- Hogan, J.D., Keenan, J.L., Luo, L., Ibn-Salem, J., Lamba, A., Schatzberg, D., Piacentino, M.L., Zuch, D.T., Core, A.B., Blumberg, C., Timmermann, B., Grau, J.H., Speranza, E., Andrade-Navarro, M.A., Irie, N., Poustka, A.J., Bradham, C.A., 2020. "The developmental transcriptome for *Lytechinus variegatus* exhibits temporally punctuated gene expression changes." *Developmental Biology* 460 (2): 139-154.
- Kim, Y., Ganesan, K., Yang, P., Kulak, A.N., Borukhin, S., Pechook, S., Ribeiro, L., Kroeger, R., Eichhorn, S.J., Armes, S.P., Pokroy, B., Meldrum, F.C., 2011. "An artificial biomineral formed by incorporation of copolymer micelles in calcite crystals." *Nature Materials* 10 (11): 890-896.
- Kipryushina, Y.O., and Yakovlev, K.V., 2020. "Maternal Control of Early Patterning in Sea Urchin Embryos." *Differentiation (London)* 113: 28-37.
- Li, E., Cui, M., Peter, I.S., Davidson, E.H., 2014. "Encoding regulatory state boundaries in the pregastrular oral ectoderm of the sea urchin embryo." *Proceedings of the National Academy of Sciences* 111 (10): 906-913.

- Logan, C.Y., Miller, J.R., Ferkowicz, M.J., McClay, D.R., 1999. "Nuclear Beta-Catenin Is Required to Specify Vegetal Cell Fates in the Sea Urchin Embryo." *Development (Cambridge)* 126 (2): 345-357.
- Lyons, D.C., Kaltenbach, S.L., McClay, D.R., 2011. "Morphogenesis in sea urchin embryos: linking cellular events to gene regulatory network states." *Developmental biology* 1 (2): 231-252.
- Lyons, D.C., Martik, M.L., Saunders, L.R., McClay, D.R., 2014. "Specification to Biomineralization: Following a Single Cell Type as It Constructs a Skeleton." *Integrative and Comparative Biology* 54 (4): 723-733.
- McClay, D.R., Fink, R.D., 1982. "Sea Urchin Hyalin: Appearance and Function in Development." *Developmental Biology* 92 (2): 285-293.
- McIntyre, D.C., Lyons, D.C., Martik, M., McClay, D.R., 2014. "Branching out: Origins of the Sea Urchin Larval Skeleton in Development and Evolution." *Genesis* 52 (3): 173-185.
- McIntyre, D.C., Seay, N.W., Croce, J.C., McClay, D.R., 2013. "Short-Range Wnt5 Signaling Initiates Specification of Sea Urchin Posterior Ectoderm." *Development (Cambridge)* 140 (24): 4881-4889.
- Miller, J., Fraser, S.E., McClay, D.R., 1995. "Dynamics of Thin Filopodia during Sea Urchin Gastrulation." *Development (Cambridge)* 121 (8): 2501-2511.
- Nassif, N., Pinna, N., Gehrke, N., Antonietti, M., Jager, C., Colfen, H., 2005. "Amorphous Layer around Aragonite Platelets in Nacre." *Proceedings of the National Academy of Sciences* 102 (36): 12653-12655.
- Neues, F., Ziegler, A., Epple, M., 2007. "The composition of the mineralized cuticle in marine and terrestrial isopods: A comparative study." *CrystEngComm* 9 (12): 1245-1251.
- Oliveri, P., Carrick, D.M., Davidson, E.H., 2002. "A regulatory gene network that directs micromere specification in the sea urchin embryo." *Developmental Biology* 246: 209-228.
- Oliveri, P., Davidson, E.H., McClay, D.R., 2003. "Activation of pmar1 controls specification of micromeres in the sea urchin embryo." *Developmental Biology* 258 (1): 32-43.
- Piacentino, M.L., Zuch, D.T., Fishman, J., Rose, S., Speranza, E.E., Li, C., Yu, J., Chung, O., Ramachandran, J., Ferrell, P., Patel, V., Reyna, A., Hameeduddin, H., Chaves, J.,

- Hewitt, F. B., Bardot, E., Lee, D., Core, A.B., Hogan, J.D., ... Bradham, C.A., 2016. "RNA-Seq Identifies SPGs as a Ventral Skeletal Patterning Cue in Sea Urchins." *Development (Cambridge)* 143 (4): 703-714.
- Range, R.C., 2018. "Canonical and Non-Canonical Wnt Signaling Pathways Define the Expression Domains of Frizzled 5/8 and Frizzled 1/2/7 along the Early Anterior-Posterior Axis in Sea Urchin Embryos." *Developmental Biology* 444 (2): 83-92.
- Range, R.C., Angerer, R.C., Angerer L.M., 2013. "Integration of Canonical and Noncanonical Wnt Signaling Pathways Patterns the Neuroectoderm Along the Anterior-Posterior Axis of Sea Urchin Embryos." *PLoS Biology* 11 (1): e1001467.
- Range, R.C., Wei, Z., 2016. "An Anterior Signaling Center Patterns and Sizes the Anterior Neuroectoderm of the Sea Urchin Embryo." *Development (Cambridge)* 143 (9): 1523-1533.
- Razinia, Z., Carroll, E.J., Oppenheimer, S.B., 2007. "Microplate Assay for Quantifying Developmental Morphologies: Effects of Hyalin on Sea Urchin Gastrulation." *Zygote* 15 (2): 159-164.
- Roberson, M., Oppenheimer, S.B., 1975. "Quantitative Agglutination of Specific Populations of Sea Urchin Embryo Cells with Concanavalin A." *Experimental Cell Research* 91 (2): 263-268.
- Robinson, J.J., 1988. "Roles for Ca²⁺, Mg²⁺ and NaCl in Modulating the Self-Association Reaction of Hyalin, a Major Protein Component of the Sea-Urchin Extraembryonic Hyaline Layer." *Biochemical Journal* 256 (1): 225-28.
- Sawada, M., Sridhar, K., Kanda, Y., Yamanaka, S., 2021. "Pure hydroxyapatite synthesis originating from amorphous calcium carbonate." *Scientific Reports* 11 (1): 11546.
- Smotrina, T.V., Severin, A.V., Shcheglova, N.V., 2019. "Sorption Interaction with Water of Hydroxyapatite, Hyaluronic Acid, and β -Casein, Individual Components of Synthetic Biomineral Compositions." *Polymer Science Series B* 61 (4): 442-450.
- Sun, H., Peng, C.J., Wang, L., Feng, H., Wikramanayake, A.H., 2021. "An Early Global Role for Axin Is Required for Correct Patterning of the Anterior-Posterior Axis in the Sea Urchin Embryo." *Development (Cambridge)* 148 (7): dev191197.
- Sun, Z., Etensohn, C.A., 2014. "Signal-Dependent Regulation of the Sea Urchin Skeletogenic Gene Regulatory Network." *Gene Expression Patterns* 16 (2): 93-103.

- Weiss, I.M., Tuross, N., Addadi, L., Weiner, S., 2002. "Mollusc larval shell formation: amorphous calcium carbonate is a precursor phase for aragonite." *The Journal of Experimental Zoology* 293 (5): 478-491.
- Wessel, G.M., Berg, L., Adelson, D.L., Cannon, G., McClay, D.R., 1998. "A Molecular Analysis of Hyalin - A Substrate for Cell Adhesion in the Hyaline Layer of the Sea Urchin Embryo." *Developmental Biology* 193 (2): 115-126.
- Wu, C., Park, A., Joester, D., 2011. "Bioengineering Single Crystal Growth." *Journal of the American Chemical Society* 133 (6): 1658-1661.
- Xiao, C., Li, M., Wang, B., Liu, M., Shao, C., Pan, H., Lu, Y., Xu, B., Li, S., Zhan, D., Jiang, Y., Tang, R., Liu, X.Y., Colfen, H., 2017. "Total morphosynthesis of biomimetic prismatic-type CaCO₃ thin films." *Nature Communications* 8 (1): 1-9.
- Yaguchi, S., Yaguchi, J., Burke, R.D., 2006. "Specification of ectoderm restricts the size of the animal plate and patterns neurogenesis in sea urchin embryos." *Development (Cambridge)* 133 (12): 2337-2346.
- Yaguchi, S., Yaguchi, J., Burke, R.D., 2007. "Sp-Smad2/3 mediates patterning of neurogenic ectoderm by nodal in the sea urchin embryo." *Developmental Biology* 302 (2): 494-503.
- Yuh, C., Dorman, E.R., Howard, M.L., Davidson, E.H., 2004. "An otx cis-regulatory module: a key node in the sea urchin endomesoderm gene regulatory network." *Developmental Biology* 269 (2): 536-551.
- Zhao, Y., Sun, B., Wang, T., Yang, L., Xu, X., Chen, C., Wei, F., Lv, W., Zhang, L., Sun, D., 2019. "Synthesis of cellulose-silica nanocomposites by in situ biomineralization during fermentation." *Cellulose (London)* 27 (2): 703-712.
- Zuch, D.T., Bradham, C.A., 2019. "Chapter 18 - Spatially Mapping Gene Expression in Sea Urchin Primary Mesenchyme Cells." *Methods in Cell Biology* 151: 433-442.
- Zuch, D.T., Hawkins, D., Huth, J., Rose, S., Lamba, A., Dionne, K., Li, C., Murray, I., Patel, V., Piacentino, M.L., Bradham, C.A., 2022. "Lipoxygenase is a Developmental Skeletal Patterning Cue." (in revision)

CURRICULUM VITAE

